Plasma effects on atomic reaction rates in hydrogen plasmas

Jun Li and Yukap Hahn
Physics Department, University of Connecticut, Storrs, Connecticut 06269
(Received 30 April 1993)

The perturbative effects of plasma electrons and ions on the effective capture and ionization rates in hydrogen plasma are analyzed. A simple model of hydrogen plasma is constructed to extract the salient features of the system, which is assumed to be in local thermal equilibrium. The interplay between the collisional and radiative processes as functions of the electron temperature and density is explicitly demonstrated. A large increase in the collisional radiative recombination rates at high density and low temperature is caused by (i) the shift in the dominant capture mechanism from the radiative to collisional cascade, and (ii) the presence of upper states in Saha equilibrium which act as a reservoir of population flux. Different sets of effective rates which reflect the approximate structure of the rate equations are evaluated, stressing the relationship between the rate coefficients and the rate equations. When the angular-momentum sublevels are averaged over, because of rapid l-changing collisions, the ion field distortion effect is shown to be negligible, in the lowest order approximation.

PACS number(s): 52.20.−j, 52.70.−m

I. INTRODUCTION

Much work has been done in recent years in generating various reaction rates for different ionic species which are present inside plasmas, for modeling and diagnostics of low-temperature industrial plasmas as well as high-temperature fusion and astrophysical plasmas. In almost all cases, the rates for electron-ion collisional excitation, ionization, and capture have been calculated in the zero-density limit and for the ground states. Local thermal equilibrium (LTE) is also assumed for the electron-ion distributions in calculating the rates. As stressed recently [1], some of these assumptions are not applicable in many practical cases, and we list below several critical factors that require careful analyses:

(a) The plasma effects on atomic reaction rates can be very large [2–15]. The plasma effects involve both field distortion (FD) of the atomic (or ionic) states [4–7], primarily caused by the plasma ion perturbers, and collisional transitions (CT) among the atomic levels, caused mainly by the plasma electrons [9–11]. The FD and CT effects are often inseparable and must be treated simultaneously. The rate equations deal with the CT effect, while the input rates and the very definition of the states that the CT connect are affected by the FD effect.

(b) When the rate equations contain more than one atomic state, the required input data are obviously those rates for the ground states as well as for the excited states included explicitly in the truncated set of rate equations. Thus, the definition of rates must reflect the structure of the rate equations being used. This is a rather trivial point but one that has often been ignored in generating the rate data.

(c) In addition to the principal elements of a plasma, e.g., electron and protons in hydrogen plasma, there are almost always other impurity ions which can seriously disrupt the various atomic processes, including ion-atom collisions with or without charge exchange.

(d) Actual plasmas are not always in LTE, even within a limited small volume inside the plasma, due to the transport of particles and turbulence [12]. Plasma container walls and external particle injections, etc., produce non-Maxwellian distributions and can seriously affect the rates themselves, which are defined in terms of the distribution function f.

It is therefore desirable to formulate the modeling problem in a systematic way [13–16], consistently taking into account all the critical factors and assumptions. As a first step in this effort, we consider the CT and FD effects for the simple system of hydrogen plasma [2], concentrating on points (a) and (b) discussed above. Points (c) and (d) are important, but will not be considered in this paper. They will be treated in later reports [17].

Hydrogen plasma is obviously the simplest system and was studied in the pioneering work of Bates *et al.* [2], where the collisional radiative recombination and ionization rates were shown to change many orders of magnitudes from the direct radiative recombination and direct ionization rates, especially at high densities and at low temperatures. These results involve several critical assumptions introduced in the theory, and it is the purpose of this paper to analyze the system further, in terms of a simple model. As will be shown in Sec. IV, the model contains three levels, with all the essential features of the original system, and can even predict the rates quantitatively at high densities. The model is used to examine both points (a) and (b) raised above.

In Sec. II we summarize the original theory of Bates *et al.*, and list carefully the critical assumptions which were introduced. A simple three-level model will be constructed in Sec. III. A numerical study of the model will be presented in Sec. IV, where different approximations on the excited-state populations are shown to change the final solutions, thus further clarifying the role played by the excited states which are in Saha equilibrium. The effect of ionic field perturbation and the l mixing is briefly considered in Sec. V. The angular-momentum dependence has been averaged over in the original system, and

we will show that the main FD effect may be minimal in the l-averaged theory.

Extensions of the present study to include the angular-momentum dependence and corresponding field distortion effect, and the contribution of the closely packed Rydberg states, will be considered in future works. The FD effect on high Rydberg states (HSR) may be conveniently treated by a quasicontinuum model in terms of Fokker-Planck equations [9,10,17].

As noted in (c) above, high-temperature plasmas often contain a sizable amount of heavy impurities. These impurities with varying degrees of ionization introduce complex atomic processes involving more than one electron, such as the dielectronic recombination, resonant excitation and autoionization, etc. The resonant processes involving high Rydberg states are especially sensitive to plasma effects. The hydrogen-plasma model we study here focuses more on the basic structure of the problem without the complications of heavier ions and resonances. But eventually more complex ionic structure allows investigation of points (c) and (d) above [11–15].

II. THE HYDROGEN PLASMA

We first summarize briefly the hydrogen plasma studied by Bates *et al.* [2], using their notation. The physical assumptions and approximations introduced in the construction and solution of the rate equations will be explicitly enumerated. This will lead naturally to our model presented in Sec. III.

The rate equations for the number densities n_p of hydrogen atoms in states p are given by

$$\dot{n}_p = -n_p \left[n_c \left[K_{pc} + \sum_{q\,(\neq p)} K_{pq} \right] + \sum_{q\,(<p)} A_{pq} \right] + n_c \sum_{q\,(\neq p)} n_q K_{qp} + \sum_{q\,(>p)} n_q A_{qp} + n_c n_I [K_{cp} + \beta_p] , \tag{1}$$

where K_{cp} are collisional (three-body) recombination rates, from $c \to p$, which are density dependent. The density-independent rates are $\tilde{K}_{cp}$ ($\tilde{K}_{cp} \equiv K_{cp}/n_c$). The collisional ionization rates, from $p \to c$, are K_{pc}. The collisional excitation or deexcitation rates, from $p \to q$, are K_{pq}. The radiative decay rates, from $p \to q$, with $p > q$, are A_{pq}. The radiative recombination rates, $c \to p$, are β_p.

Several critical assumptions were introduced in the construction of (1) which are summarized below:

(i) The continuum electron density n_c and the ion density n_I are held constant throughout the duration of relaxation, independent of the initial conditions, even when the atomic population is much larger than that of free electrons and ions. This implies that we have infinitely large electron and ion baths of the surrounding plasma that maintain the overall electron and ion densities in the specified local volume, within which we assume the plasma in local thermal equilibrium insofar as the continuum particles are concerned, with constant densities. (For neutral plasmas, we also have $n_c = n_I$.) Extensions of this approximation where n_c and n_I vary in time are not readily solvable because of the nonlinearity of the rate equations for these quantities.

(ii) The l sublevels are averaged over to simplify the treatment. This is partially justified when the l-mixing collisions by the plasma particles are very fast, effectively populating all the l sublevels statistically. This is reasonable and greatly simplifies the analysis. All the rates which appear in (1) have been properly adjusted. Some discussion on this problem is given in Sec. V in connection with the field distortion effect. The problem of explicit l dependence and field mixing will be considered in detail elsewhere [18].

(iii) The plasma is assumed to be optically thin, so that all the radiation emitted escape the local volume, draining energy from the plasma. Furthermore, all the heavy-particle collisions are neglected; this is consistent with assumption (ii) above. There are, of course, many cases in which such simplifications cannot be made, especially when impurity ions are present, with strong charge-exchange channels, and for a plasma microsphere deep inside a dense plasma (optically dense), as in the interior of the sun.

(iv) For high Rydberg states with $p > s$, for some s to be specified later, the nearest-neighbor collisional transitions dominate, and the number density n_p may be assumed to have reached the Saha equilibrium at all times. The structure of (1) and the Maxwell distribution assumed for the electrons in LTE are consistent with the assumption that when p is large enough, all the radiative processes are negligible and collisional processes dominate.

The population density may be normalized in terms of the Saha equilibrium values where

$$n_p^E = n_c n_I p^2 \left[\frac{2\pi\hbar^2}{m k_B T_c} \right]^{3/2} \exp(I_p/k_B T_e) , \tag{2}$$

where I_p is the ionization energy of the state p.

It is convenient to normalize n_p in terms of the Saha values as

$$P_p(t) \equiv n_p / n_p^E , \tag{3}$$

such that we have by the definition of s,

$$P_p = 1 \quad \text{for } p > s . \tag{4}$$

The detailed balance relations at equilibrium, as a result of time-reversal invariance of the collision cross sections, are given by

$$n_q^E K_{qp} = n_p^E K_{pq} \quad \text{and} \quad n_I K_{cp} = n_p^E K_{pc} , \tag{5}$$

which are also consistent with the Saha equilibrium values (2).

The rate equations in terms of the normalized population densities P replace (1). Using (5) and the explicit equilibrium densities inserted to adjust the rates, we can rewrite (1) as

$$\dot{P}_p = -P_p \left[n_c \left[K_{pc} + \sum_{q\,(\neq p)} K_{pq} \right] + \sum_{q\,(<p)} A_{pq} \right] + \sum_{q\,(\neq p)} P_q n_c K_{pq} + \sum_{q\,(>p)} P_q (n_q^E/n_p^E) A_{qp} + n_c K_{pc} + (n_c n_I / n_p^E) \beta_p \tag{6}$$

for p and $q \leq s$. The actual values of s, where $P_p \rightarrow 1$ for all $p > s$, depend on the electron density and temperature, and are determined iteratively by observing the solutions of (6) as a function of p. This is discussed further in Sec. IV. The property that $P_p \simeq 1$, $p > s$ allows one to truncate the infinite set of coupled rate equations (6) to a finite set of s equations.

When the system described by (6) reaches the equilibrium (i.e., $\dot{P}_p = 0$), the solution does not depend on the initial conditions, because (6) is linear and inhomogeneous in P. The equilibrium properties for the states $p \leq s$ are obtained by first setting in (6) $\dot{P}_{p'} = 0$ for all $p' > 1$, and excluding the ground state $p = 1$. Following Ref. [2], we write

$$P_{p'} = r_{0p'} + r_{1p'} P_1 , \quad p' > 1 . \tag{7}$$

Substitution of (7) into the P_1 equation eliminates all the $P_{p'}$ and we obtain

$$\dot{P}_1 = (n_c n_l / n_1^E)\alpha_1 - n_c S_1 P_1 . \tag{8}$$

The physical interpretation of this result is that if one were to describe the hydrogen plasma in terms of the single ground-state equation (8), the effective rate coefficients to be inserted are the collisional radiative recombination α_1 and collisional radiative ionization rate S_1. Substitution of the solution of Eq. (8) for P_1 into (7) gives all the other $P_{p'}$ as functions of t. For later discussion it is convenient to define separately the radiative and collisional contributions as

$$S_1 = S_{1c} - S_{1r} , \tag{8'}$$

where the minus sign in front of S_{1r} is introduced to make the S_{1r} positive. In addition, we also set

$$\alpha_1 = \alpha_{1c} + \alpha_{1r} . \tag{8''}$$

Next, the solution for P_1 at equilibrium is obtained by setting $\dot{P}_1 = 0$ in (8), and we obtain

$$P_1^E = n_l \alpha_1 / (n_1^E S_1) , \tag{9}$$

which is in general different from unity. But, at high densities the collisional effect dominates, leading to $P_1^E \rightarrow 1$. When (9) is put back to (7), we obtain the equilibrium population of the excited states:

$$P_{P'}^E = r_{0p'} + r_{1p'} n_l \alpha_1 / (n_1^E S_1) , \quad p' > 1 . \tag{10}$$

All the input rates which appear in Eqs. (1) and (6) are given in the various references [6–9]. We summarize in Table I only those values which are needed in the study of the model to be presented in Sec. III. All the other quantities which appear in Eqs. (7)–(10) are expressed in terms of these input rates. Their explicit formulas are complex, but in Sec. III, a simple model will be constructed, and all the derived states are readily given explicitly.

TABLE I. The collisional and radiative rates used in the model are summarized at three temperatures: (a) K_{pq} are the collisional rates for $p \rightarrow q$ transitions, given in units of cm^3/sec. The inverse rates $\tilde{K}_{cp}$, in units of cm^6/sec, are given in the row immediately below the direct rates. The large difference in magnitudes between the direct and inverse rates at low T is due to the Saha equilibrium values and extra density factor, as shown in (2) and (5). (b) β_p are the radiative recombination rates to state p from the continuum. (c) A_{pq} are the spontaneous radiative decay probabilities for the transitions $p \rightarrow q$. The electron density n_c is given in units of cm^{-3}, and the rates are in cm^3/sec. Numbers in square brackets denote powers of 10.

(a) Collisional rates

T (10^3 K)	K_{12}/K_{21}	K_{13}/K_{31}	K_{23}/K_{32}	K_{34}/K_{43}	$K_{1c}/\tilde{K}_{c1}$	$K_{2c}/\tilde{K}_{c2}$	$K_{3c}/\tilde{K}_{c3}$
4	4.82[−21]	4.20[−24]	2.69[−09]	5.68[−07]	1.34[−26]	2.73[−12]	4.19[−09]
4	8.66[−09]	8.07[−10]	2.87[−07]	2.18[−06]	3.09[−30]	3.50[−28]	5.02[−27]
16	2.17[−11]	1.14[−12]	1.82[−07]	2.73[−06]	3.38[−13]	1.23[−08]	2.38[−07]
16	8.89[−09]	8.17[−10]	3.19[−07]	2.48[−06]	1.36[−30]	1.20[−28]	1.33[−27]
64	5.83[−09]	8.31[−10]	5.17[−07]	3.58[−06]	1.54[−09]	1.33[−07]	6.74[−07]
64	9.29[−09]	8.27[−10]	3.24[−07]	2.27[−06]	4.70[−31]	2.55[−29]	2.07[−28]

(b) Radiative recombination rates

T (10^3K)	β_1	β_2	β_3	β_4	β_5	β_6	β_7
4	2.50[−13]	1.32[−13]	8.44[−14]	5.86[−14]	4.29[−14]	3.26[−14]	2.54[−14]
16	1.20[−13]	5.63[−14]	3.19[−14]	2.00[−14]	1.35[−14]	9.56[−15]	7.06[−15]
64	5.19[−14]	1.95[−14]	9.48[−15]	5.37[−15]	3.36[−15]	2.25[−15]	1.59[−15]

(c) Spontaneous radiative decay probabilities A_{pq}

p \ q	1	2	3	4	5	6	7
2	4.70[8]						
3	5.58[7]	4.41[7]					
4	1.28[7]	8.42[6]	8.99[6]				
5	4.13[6]	2.53[6]	2.20[6]	2.70[6]			
6	1.64[6]	9.74[5]	7.79[5]	7.72[5]	1.03[6]		
7	7.57[5]	4.39[5]	3.36[5]	3.04[5]	3.25[5]	4.56[5]	
8	3.87[5]	2.22[5]	1.65[5]	1.42[5]	1.39[5]	1.56[5]	2.27[5]

III. A THREE-LEVEL MODEL

In order to bring out the essential features of the hydrogen plasma described by (1) and (6), we consider a simple three-level atom of the hydrogen plasma in LTE, i.e., the states $1+2+3+c$ (continuum). All the quantities can then be explicitly written down and various effects identified.

A. The model

The rate equations for the population of these states are given by

$$\dot{P}_1 = -P_1[n_c K_{1c} + n_c K_{12} + n_c K_{13}] + P_2 n_c K_{12} + n_c K_{13} P_3 + P_2 (n_2^E / n_1^E) A_{21} + (n_3^E / n_1^E) A_{31} P_3 + n_c K_{1c} + (n_c^2 / n_1^E)\beta_1 , \tag{11a}$$

$$\dot{P}_2 = -P_2[n_c K_{2c} + n_c K_{21} + n_c K_{23} + A_{21}] + n_c K_{21} P_1 + n_c P_3 K_{23} + (n_3^E / n_2^E) A_{32} P_3 + n_c K_{2c} + (n_c^2 / n_2^E)\beta_2 , \tag{11b}$$

$$\dot{P}_3 = -P_3[n_c K_{3c} + n_c K_{31} + n_c K_{32} + A_{31} + A_{32}] + n_c K_{31} P_1 + n_c P_2 K_{32} + n_c K_{3c} + (n_c^2 / n_3^E)\beta_3 . \tag{11c}$$

As will be shown, the effectiveness of the model comes from the fact that when level p with $p > s$ is depleted by collisions and radiative decays, they are instantly repopulated to Saha equilibrium. This feature of the model thus provides an unlimited source of electrons in the excited states, so that whether we have many upper levels or just one level 3, the final effect on states 1 and 2 is similar. Somewhat simpler models involving one and two bound levels are also considered in Appendixes A and B, respectively.

There are many ways by which initial conditions may be chosen, and these give different solutions. The construction of the desired model is complete with the final assumption that

$$P_3 = 1 . \tag{12}$$

Choice (12) is somewhat arbitrary and the effective P_3 may lie between 0 and 2 when (6) is fully solved. Its value depends on the electron temperature and density. Therefore, this number may be adjusted as a parameter at this stage. Since level 3 presumably represents all the states which lie above it, (12) should be regarded as an effective value. With (12), Eqs. (9) are essentially reduced to that for P_1 and P_2 only, as

$$\dot{P}_1 = -P_1[n_c K_{1c} + n_c K_{12} + n_c K_{13}] + P_2 n_c K_{12} + n_c K_{13} + P_2 (n_2^E / n_1^E) A_{21} + (n_3^E / n_1^E) A_{31} + n_c K_{1c} + (n_c^2 / n_1^E)\beta_1 , \tag{13a}$$

$$\dot{P}_2 = -P_2[n_c K_{2c} + n_c K_{21} + n_c K_{23} + A_{21}] + n_c K_{21} P_1 + n_c K_{23} + (n_3^E / n_2^E) A_{32} + n_c K_{2c} + (n_c^2 / n_2^E)\beta_2 . \tag{13b}$$

Equations (13) define our model, whose properties we will study numerically in the Sec. IV. As will be shown, assumption (12) has a profound effect on the final equilibrium population of states 1 and 2. We note in particular that the terms $n_c K_{13}$ in (13a) and $n_c K_{23}$ in (13b) retain the trace of state 3, and become dominant at high density.

B. $\dot{P}_2 = 0$, $P_3 = 1$

Equation (13) may be reduced for $\dot{P}_1$ alone at equilibrium by setting the left-hand side of (13b) equal to 0, and we obtain equations similar to (8). Thus, from (13b) we have

$$P_2 = D_2^{-1} n_c K_{21} P_1 + D_2^{-1}[n_c K_{23} + (n_1^E / n_2^E) A_{32} + n_c K_{2c} + (n_c^2 / n_2^E)\beta_2] , \tag{14}$$

where

$$D_2 \equiv n_c[K_{2c} + K_{21} + K_{32}] + A_{21} .$$

Substitution of (14) into (13a) then gives

$$\dot{P}_1 = (n_c n_1 / n_1^E)\alpha_1^{(3)} - n_c S_1^{(3)} P_1 , \tag{15}$$

where we have explicitly

$$\alpha_1^{(3)} = \{K_{c1} + n_3^E K_{31}/n_c + [K_{c2} + n_3^E K_{32}/n_c] D_2^{-1} n_c K_{21}\} + \{\beta_1 + [\beta_2 + n_3^E A_{32}/n_c^2] D_2^{-1} A_{21} + [K_{c2} + n_3^E K_{32}/n_c] D_2^{-1} A_{21} + [\beta_2 + n_3^E A_{32}/n_c^2] D_2^{-1} n_c K_{21}\} \equiv \alpha_{1c}^{(3)} + \alpha_{1r}^{(3)} , \tag{16a}$$

$$S_1^{(3)} = \{K_{1c} + K_{13} + K_{12} - K_{12} D_2^{-1} n_c K_{21}\} - K_{12} D_2^{-1} A_{21} \equiv S_{1c}^{(3)} - S_{1r}^{(3)} . \tag{16b}$$

In (16), as in (8′) and (8″), we separated the collisional and radiative contributions by putting all the terms that contain the radiative part in "r," and the collisional part in "c," except for the D factor. The numerical values for the effective capture and ionization rates $\alpha_1^{(3)}$ and $S_1^{(3)}$, respectively, are tabulated in Table III (a). This is one of the main results of this paper and can be compared with the result of Bates *et al.* [2].

C. $\dot{P}_2 \neq 0, P_3 = 1$

For transient solutions, we have directly from (11) a coupled set of equations,

$$\dot{P}_1 = -n_c S_l^{(3)'} P_1 + (n_c n_l / n_1^E)\alpha_1^{(3)'} + X_{12} P_2 \ , \tag{17a}$$

$$\dot{P}_2 = -n_c S_2^{(3)'} P_2 + (n_c n_l / n_2^E)\alpha_2^{(3)'} + X_{21} P_1 \ , \tag{17b}$$

where the various factors are immediately identified from (16). In particular, we have

$$X_{12} = n_c K_{12} + (n_2^E / n_1^E) A_{21} \ , \tag{18a}$$

$$X_{21} = n_c K_{21} \ . \tag{18b}$$

As will be shown in Sec. IV, $S_1^{(3)'}$ and $\alpha_1^{(3)'}$ are different from $S_1^{(3)}$ and $\alpha_1^{(3)}$ of (15), stressing the point that the effective rates S and α have to reflect the specific form of the rate equations.

D. Other approximations

Instead of condition (12), we may directly solve (11) by taking the following options:

(i) $P_3 \simeq P_2 \simeq 0$. This reduces to the one-level model of Appendix A.

(ii) $P_3 \simeq 0$, which reduces the model to that of two levels discussed in Appendix B. Two cases $P_2 = 1$ and $\dot{P}_2 = 0$ are possible.

(iii) $\dot{P}_2 = \dot{P}_3 = 0$. We then obtain from (11) an equation for the ground state $p = 1$ similar to (8). Here we do not assume (12).

(iv) $\dot{P}_3 \simeq 0$. This provides a coupled set of equations for the transient solutions for the two lowest states, but as with all the above, the absence of (12) is a serious shortcoming of this approximation, as will be seen in Sec. IV.

In all of the above four cases, the behavior of the plasma is quite different from that of (13) with (12), illustrating the importance of condition (12). Thus, the useful features of our model are that (a) the role of the excited states with $p > 2$ is compactly represented by (12), (b) cascade contributions from and to level 3 through level 2 are included, (c) the distinction between the effective rates with and without level 2 is brought out clearly, and (d) the radiative and collisional contributions can be explicitly demonstrated.

IV. NUMERICAL RESULTS

We numerically examine the model defined by (13), and the other approximate models introduced in Secs. II and III. The effective rates at equilibrium are explicitly evaluated and compared with the solutions of Eq. (6).

A. The full system of Bates *et al.*

We start with the solution of the full system described by (1) and (6) of Sec. II. The solution is, of course, identical to that of Bates *et al.* [2] when all the input rates used are the same, but the result is presented here in a form that is convenient for comparison with the following model solutions.

First, the input rates for Eq. (6) are needed. They are obtained from Refs. [19–21] and are l averaged, consistent with the rate equations. Table I contains the collisional transition rates K_{pq} for $p,q \lesssim 4$, the collisional ionization rates K_{pc} and their inverse K_{cp}, and the three-body recombination rates. Table I, part (b), gives the radiative recombination rates β_p, for $p < 8$. Both these quantities depend on the electron temperature T. Finally, Table I part (c), summarizes the radiative decay probabilities A_{pq}, with $p > q$, for $p, q < 9$.

The set of coupled equations (6) are solved by setting $\dot{P}_p = 0$ for all $p > 1$, after truncating the set at $p = s$. The states with $p > s$ have reached the Saha equilibrium at all times. The parameter s depends on the density and temperature, and generally $s < 30$. Depending on the desired accuracy of the solution, say, one part in 10 000, the s was determined by solving the set for P with an initial s and checking iteratively for the resulting $P_s \simeq 1$ to a preset accuracy. The result is given in Table II, which used a more complete set of rates than that given in Table I.

TABLE II. The effective collisional radiative recombination and ionization rates α_1 and S_1, respectively, are given, as defined by Eq. (8) for the full system (6). The collisional and radiative contributions are listed separately (subscripts c and r). Note the shift in the dominance as the electron density is increased. These rates are to be compared with the direct rates given in Table I. The approximate model solutions of this paper are also compared with this table. The cutoff values s are given in the last column. They are determined numerically by testing the values of P_p such that the population densities approach unity for all $p > s$, to a preset accuracy. The density and temperature dependence of this parameter is evident. The small s at high density is reflected in the goodness of the three-level model, where $P_3 = 1$ was assumed. Numbers in square brackets denote powers of 10.

$\log_{10} n_c$	T (10^3 K)	S_{1c}	S_{1c}	S_1	α_{1c}	α_{1c}	α_1	s
8	4	4.8[−21]	4.8[−21]	1.1[−26]	1.5[−21]	9.8[−13]	9.8[−13]	20
8	16	2.4[−11]	2.3[−11]	3.7[−13]	4.5[−22]	3.1[−13]	3.1[−13]	7
8	64	8.8[−09]	7.3[−09]	1.6[−09]	1.3[−22]	1.0[−13]	1.0[−13]	4
13	4	4.8[−21]	4.8[−21]	3.6[−25]	2.0[−15]	1.3[−11]	1.3[−11]	18
13	16	2.4[−11]	2.3[−11]	1.1[−12]	9.7[−17]	6.3[−13]	6.3[−13]	5
13	64	8.8[−09]	6.4[−09]	2.4[−09]	1.6[−17]	1.2[−13]	1.2[−13]	3
18	4	1.0[−21]	2.1[−22]	8.0[−22]	1.9[−07]	1.0[−08]	2.0[−07]	15
18	16	2.3[−11]	4.2[−14]	2.3[−11]	9.2[−11]	5.0[−12]	9.7[−11]	4
18	64	8.8[−09]	3.3[−12]	8.8[−09]	2.7[−12]	1.7[−13]	2.9[−12]	3

Table II summarizes the solution of the equations (6) at equilibrium, and the effective collisional radiative ionization and recombination, S_1 and α_1, respectively, for the ground state $p=1$ are presented, as defined in (8). The collisional (c) and radiative (r) contributions are tabulated separately to show that as the electron density increases, the dominance in the rates shifts from radiative to collisional. (See also Fig. 1.) The upper-state cutoff s was determined for each density and temperature value, where the P_p are better than one part in 1.0 000 for all $p > s$.

The salient features of the solutions and the effective rates are (i) As n_c increases, the contribution to α_1 and S_1 shifts from the radiative to collisional cascades; (ii) the density effect is the largest at low T, where the collision rates are small but increase rapidly with density; (iii) the roles of excited states and cascade transitions are important. This will be brought out more clearly in the models; and (iv) For all t, the high Rydberg states with $p > s$ are in Saha equilibrium, where s is strongly dependent on T but only mildly on the density. At high T, s is very small, suggesting that, when perturbed, almost all levels quickly reach the Saha equilibrium.

B. The three-level model, with $\dot{P}_2 = 0$

Now consider the model described by (13) with the crucial approximation (12). The numerical result is given in

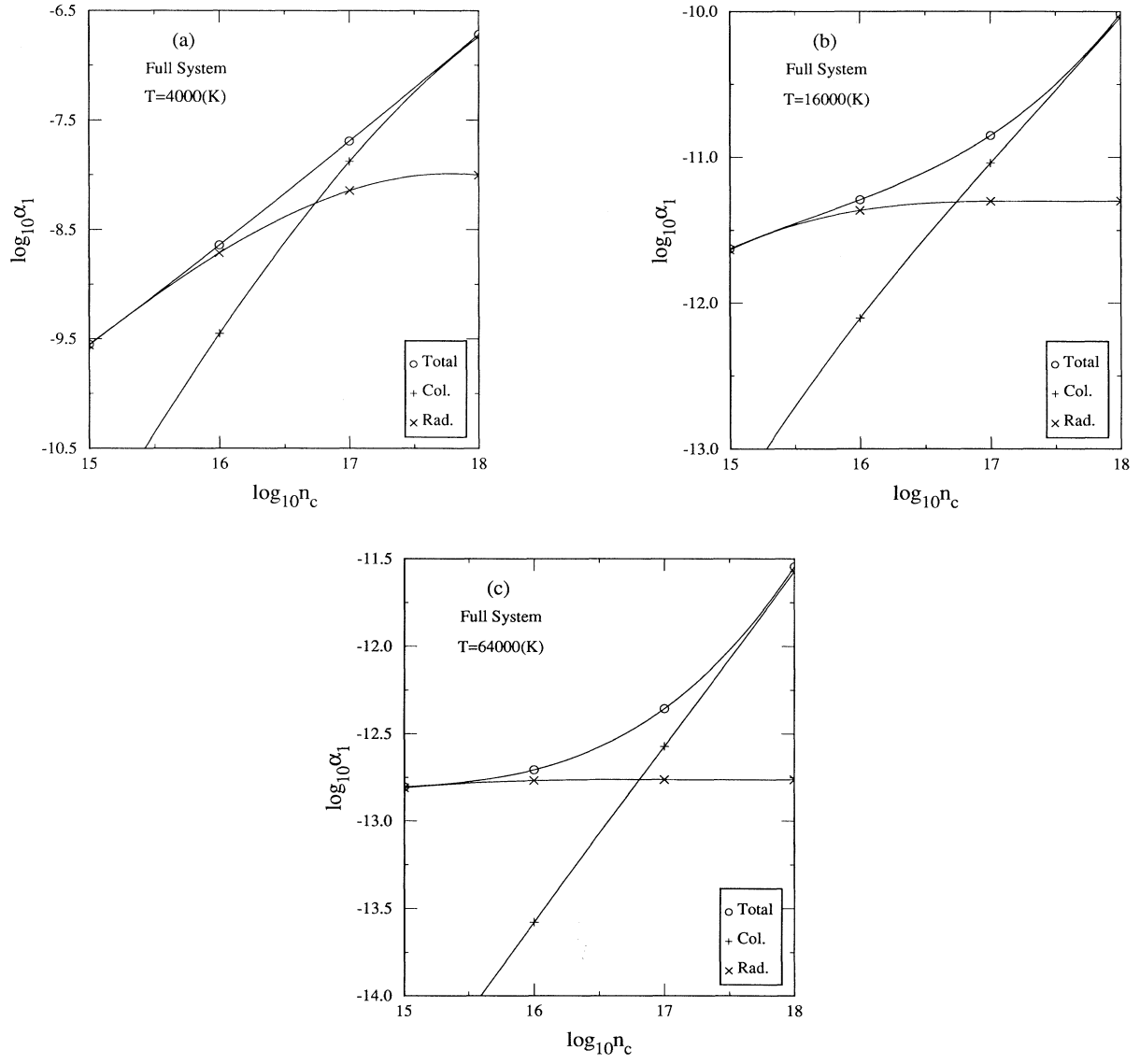

FIG. 1. The values of $\log_{10}\alpha_1$ for the full system are given as a function of electron density n_c in units of cm^{-3}. The α's are given in units of $\mathrm{cm}^3/\mathrm{sec}$. The collisional and radiative contributions are presented separately, at three different temperatures. Note that the collisional effect is small for $\log_{10} n_c < 16$. The drastic shift from the radiative to the collisional mode is seen in the figure, with the crossover at around $n_c \simeq 8\times 10^{16}\ \mathrm{cm}^{-3}$. The total rates are given by the solid line, (o).

Table III, part (a), and Fig. 2, which may be compared with that of Table II and Fig. 1(b). The qualitative trends are well reproduced for all T and n_c, and even quantitatively at high densities. Except for the low T and low density, the overall agreement with that of Table II is good. (See also Fig. 3.) The values of $S_1^{(3)}$ at low densities and low temperature are the result of severe cancellations between the two contributions c and r, and therefore their numerical values may not be very accurate.

The overestimation of the changes at low densities is due to the fact that (12) is a poor approximation of the role of all the excited states at low density. Not only does P_3 vary with T and n_c, but the presence of the rest of the excited states is being simulated by this one parameter. Nevertheless, the model is sufficiently simple to bring out the essential features of the original system. The dominant contribution to α_1 at low density is the radiative cascade mode $3\rightarrow 2\rightarrow 1$ and by the radiative recombination mode $c\rightarrow 1$, but at higher densities the collisional cascade $3\rightarrow 2\rightarrow 1$ dominates. On the other hand, for the ionization S_1, the direct ionization mode $1\rightarrow c$ is important at low densities, but the cascade excitation $1\rightarrow 2\rightarrow 3\rightarrow c$ is the main process at high density.

C. $\dot{P}_2\neq 0, P_3=1$

As stressed earlier, the effective rate coefficients must reflect the rate equations to which the rates are to be inserted. To demonstrate the point, we evaluate the effective rates of (17), and the results are given in Table III, part (b), and Fig. 3. Obviously, they are quite different from those in Table III, part (a). $S_1^{(3)'}$ and S_1 are similar only at high T and high density. On the other hand, the S's for states 1 and 2 are not easily predictable

TABLE III. The effective rates calculated using the three-level models: (a) The rates defined by Eq. (15) with assumption (12). (b) The rates defined by Eq. (17), with the same assumption (12). (c) The rates obtained without (12), as explained in Sec. III D, paragraph (iii). Numbers in square brackets denote powers of 10.

(a)

$\log_{10}n_c$	T (10^3 K)	$S_{1c}^{(3)}$	$S_{1r}^{(3)}$	$S_1^{(3)}$	$\alpha_{1c}^{(3)}$	$\alpha_{1r}^{(3)}$	$\alpha_1^{(3)}$
8	4	4.8[−21]	4.8[−21]	4.2[−24]	9.7[−20]	5.3[−11]	5.3[−11]
8	16	2.3[−11]	2.2[−11]	1.5[−12]	5.9[−22]	4.2[−13]	4.2[−13]
8	64	8.2[−09]	5.8[−09]	2.4[−09]	7.2[−23]	8.5[−14]	8.5[−14]
13	4	4.8[−21]	4.8[−21]	4.5[−24]	1.0[−14]	5.7[−11]	5.7[−11]
13	16	2.3[−11]	2.2[−11]	1.6[−12]	6.3[−17]	4.4[−13]	4.4[−13]
13	64	8.2[−09]	5.7[−09]	2.4[−09]	7.5[−18]	8.6[−14]	8.6[−14]
18	4	1.3[−21]	1.9[−22]	1.1[−21]	2.5[−07]	1.4[−08]	2.7[−07]
18	16	2.2[−11]	5.0[−14]	2.2[−11]	8.9[−11]	4.5[−12]	9.4[−11]
18	64	8.1[−09]	4.2[−12]	8.1[−09]	2.5[−12]	1.4[−13]	2.6[−12]

(b)

$\log_{10}n_c$	T (10^3 K)	$S_1^{(3)'}$	$S_2^{(3)'}$	$S_1^{(3)}$	$\alpha_1^{(3)'}$	$\alpha_2^{(3)'}$	$\alpha_1^{(3)}$
8	4	4.8[−21]	4.7[−00]	4.2[−24]	6.7[−11]	5.3[−11]	5.3[−11]
8	16	2.3[−11]	4.7[−00]	1.5[−12]	4.3[−13]	3.0[−13]	4.2[−13]
8	64	8.2[−09]	4.7[−00]	2.4[−09]	6.9[−14]	3.3[−14]	8.5[−14]
13	4	4.8[−21]	4.7[−05]	4.5[−24]	6.7[−11]	5.7[−11]	5.7[−11]
13	16	2.3[−11]	4.7[−05]	1.6[−12]	4.3[−13]	3.2[−13]	4.4[−13]
13	64	8.2[−09]	4.8[−05]	2.4[−09]	6.9[−14]	3.4[−14]	8.6[−14]
18	4	4.8[−21]	1.2[−08]	1.1[−21]	1.0[−09]	3.5[−07]	2.7[−07]
18	16	2.3[−11]	2.0[−07]	2.2[−11]	6.4[−12]	1.9[−09]	9.4[−11]
18	64	8.2[−09]	6.6[−07]	8.1[−09]	7.9[−13]	1.2[−10]	3.0[−12]

(c)

$\log_{10}n_c$	T (10^3 K)	$S_1^{(3)''}$	$S_1^{(3)}$	$\alpha_1^{(3)''}$	$\alpha_2^{(3)}$
8	4	2.0[−26]	4.2[−24]	4.7[−13]	5.3[−11]
8	16	3.4[−13]	1.5[−12]	2.1[−13]	4.2[−13]
8	64	1.5[−09]	2.4[−09]	8.1[−14]	8.5[−14]
13	4	2.4[−26]	4.5[−24]	5.2[−13]	5.7[−11]
13	16	3.7[−13]	1.6[−12]	2.2[−13]	4.4[−13]
13	64	1.6[−09]	2.4[−09]	8.2[−14]	8.6[−14]
18	4	2.2[−23]	1.1[−21]	5.2[−09]	2.7[−07]
18	16	2.1[−11]	2.2[−11]	8.9[−11]	9.4[−11]
18	64	8.1[−09]	8.1[−09]	2.6[−12]	3.0[−12]

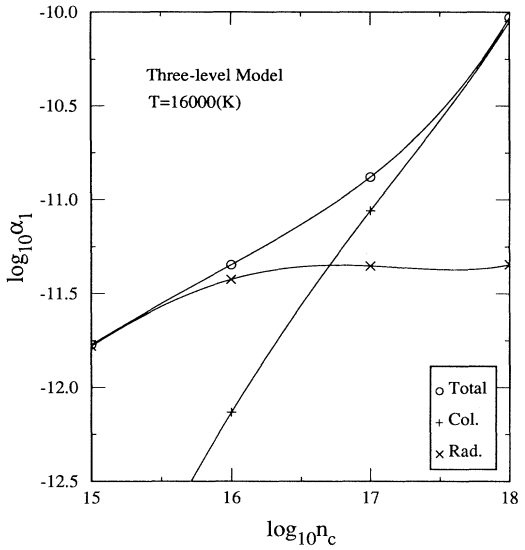

FIG. 2. One sample value of $\log_{10}\alpha_1$ obtained with the three-level model is given for $T=16\,000$ K. This figure is nearly identical to Fig. 1(b). The results for the three-level model at different temperatures are similar to that for the full system given in Fig. 1. We do not give figures for the collisional part S because of the severe cancellations among the r and c components involved.

from the general properties of the rates, unless an explicit calculation is performed, as shown here. Similar features are observed also for the α's. The steady-state solution for the ground state at $t\rightarrow\infty$ is, of course, the same as that obtained in Sec. IV B above, but the time-dependent solutions are different at finite t. Obviously, this result can be extended to the more general case where the effective rates for the truncated set of rate equations should retain the effect of states omitted in the set.

D. $\dot{P}_2=\dot{P}_3=0$

The role of the excited states, which are in Saha equilibrium at all times, can be studied by abandoning (12) and directly solving the three coupled equations (11) for all three P's, as discussed in Sec. II. The results are presented ($S_1^{(3)''}$ and $\alpha_1^{(3)''}$) in Table III part (c), and Fig. 3, which are to be compared with Table III part (a). Note the drastic reduction in the rates at low T, but the full values at higher T are quickly reached, where we expect levels 2 and 3 to be near the Saha values. The change at low T is strictly due to assumption (12); thus, the three-level model without (12) is reasonable only at high temperature, but poor at low T. The α's are less sensitive to density, while the S are not well represented at all at low density by the model without (12). This is one of the main points clarified by the model.

V. FIELD DISTORTION BY PLASMA IONS

It has been known for some time [4–7] that an electric field, external or microfield due to plasma ions, present in the atomic interaction region where reactions take place, can seriously affect the rates themselves. The plasma electron perturbers primarily cause collisional transitions, and this effect has already been included in the rate equations of types (1) and (11). On the other hand, plasma ions are relatively slow movings, and we may assume their electric field to be quasistatic, in the lowest approximation. Eventually, the strength and the direction of these fields should be averaged over their spatial and velocity distribution. In this section we assume that such an electric field is given in terms of the ion density and temperature, and consider its effect on the rates, within the l-averaged theory described in Secs. II and III.

The system described by (1) and (11) is already averaged over the angular momentum of the atomic states, as, for example,

$$A_{pq}\equiv\sum_{l_p,l_q}(2l_p+1)A(pl_p,ql_q)/p^2 \tag{19}$$

and

$$K_{pq}\equiv\sum_{l_p l_q}(2l_p+1)K(pl_p,ql_q)/p^2\ , \tag{20}$$

etc. The physical justification for this average is that once an electron is placed in the pl_p sublevel, the plasma electrons (and ions) inside the Debye sphere strongly perturb the levels and mix them uniformly over the sublevels [22] of a given principal quantum number p, since the l-changing collisions are usually very fast. Therefore, within the relaxation time of the atomic states by radiative decays, for example, it is not possible to isolate the particular initial l sublevel and retain it in that state during the decay.

The distortion of atomic states (pl_pm) of the spherical coordinate wave functions $\{\psi_{pl_pm}\}$ may be described by the corresponding solutions $\{\phi_{p\nu_pm}\}$ in the parabolic coordinates, where ν and μ are the electric quantum numbers. (We use here ν and μ in place of the usual n_1 and n_2 quantum numbers.) It was shown recently [8] that, within the subspace of degenerate levels of hydrogenic ions, one must use the spherical ψ base for $F=0$, and the parabolic ϕ basis for the field greater than some cutoff field strength equivalent of the spin-orbit coupling. The connection between the two sets is given for each p by [23–25]

$$\phi^{(p)}_{p\nu m}=\sum_{l_p}C^{(p,m)}_{\nu_p l_p}\psi_{pl_p}\ , \tag{21}$$

where the magnetic quantum number m is conserved if the field is oriented in the z direction. The coefficients C are the transformation matrix [23–27] given in terms of the Clebsch-Gordan coefficient, as

$$C^{p,m}_{\nu l}=(-1)^{1-p-m}(2l+1)^{1/2}\begin{pmatrix}p_- & p_- & l\\ m_+ & m_- & -m\end{pmatrix}, \tag{22}$$

where p is the principal quantum number of the atom, and $p_-=(p-1)/2$; $m_\pm=m\pm k$, $k=\nu-\mu$, with $\nu=1,2,\ldots,\ p-|m|-1$; and $\mu=p-\nu-|m|-1$. This formula is valid only for the subspace of given principal quantum number p, so that no mixing among the

different p's is allowed for (21) to be valid. The problem becomes more involved when the field strength is strong, so that the p- mixing is important. Recently, an approximate procedure for treating this problem was examined [8], and a simple transition operator was derived that mixed both the p and l_p. It is also possible to diagonalize the field-distorted energy matrix $\langle p|H_A+V_P|p'\rangle$ in terms of the unitary matrix C^F, analogous to C of Eq. (24). The rate equations and the rates themselves are both to be transformed using C^F, where p and q are no longer good quantum numbers.

We now evaluate the field-distorted rates in the l-averaged representation, but limiting the mixing to within a given p or q subspace. Thus by field mixing of the initial and final states in radiative decay, for example, we obtain

$$A^F_{pq}=\sum_{\nu_p,\nu_q} A(p\nu_p,q\nu_q)|\langle p\nu_p|D|q\nu_q\rangle|^2(2\nu_p+1)/p^2$$
$$\simeq \sum_{l_p,l_q}\sum_{\nu_p,\nu_q} |C^{(p)}_{l_p\nu_p}|^2|C^{(q)}_{l_q\nu_q}|^2(2\nu_p+1)A(pl_p,ql_q)/p^2$$
$$=A_{pq}\ , \tag{23}$$

where the l and ν sums were interchanged and the unitarity of the C's was used; $\sum_{\nu_p}|C^{(p)}_{l_p\nu_p}|^2=1$. D is an electric dipole coupling. Similarly, for the collisional rates by the

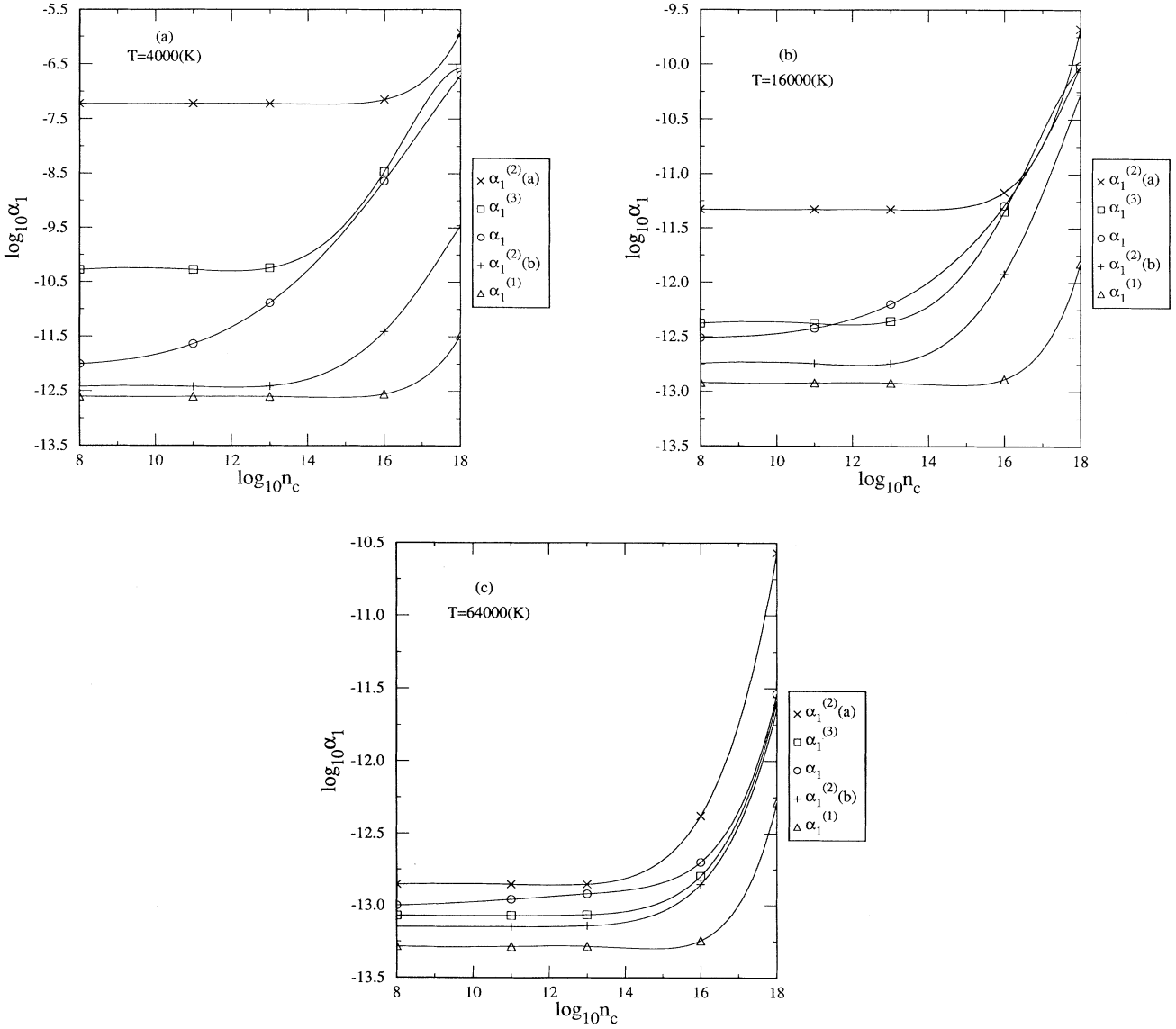

FIG. 3. The values of $\log_{10}\alpha_1$ as functions of electron density are compared for different approximate models, at three temperatures. Generally, the three-level works well for $\log_{10}n_c>15$, where the density effect starts to become significant. α_1, full model of Bates *et al*; $\alpha_1^{(3)}$, three-level model; $\alpha_1^{(2)}$(a) and $\alpha_1^{(2)}$(b), two-level model of Appendix B; $\alpha_1^{(1)}$, one-level model of Appendix A.

plasma particles (electrons), we have

$$K_{pq}^{F}=\sum_{\nu_p\nu_q}|\langle p\nu_p|V_P|q\nu_q\rangle|^2(2\nu_p+1)/p^2 \simeq K_{pq} , \quad (24)$$

where V_P is the perturbation by the plasma particles, which usually assumes a long-range–dipolelike form [13–16]. Therefore, in the l-averaged rate equations and averaged rates, the field distortion effect of the plasma ions may be neglected, to lowest order. The above proof is valid in the weak-field limit. This does not mean that the distortion effect is negligible in all cases [27]. When the explicit l dependence is retained in a more refined calculation, the field mixing by the plasma ions may turn out to be important, especially in those processes where the high Rydberg states play an important role. This problem requires further study.

VI. DISCUSSION

In this paper we have studied hydrogen plasma and showed several dominant behaviors of the solutions of the rate equations

(1) The collisional radiative recombination and ionization rates are significantly altered by the collisional transition effects caused by the plasma electrons, in complete agreement with the work of Bates *et al.* The enhancement in the rates with increasing electron density is brought about by the shift in the dominant mechanisms for capture and ionization from radiative to collisional cascades. In fact, at high densities, the capture rates become directly proportional to the electron density.

(2) The field distortion effect of the plasma ions is shown to be negligible, to lowest order and in weak-field limit, when the angular-momentum dependence has been averaged over in the theory. That is, for the field strength below the Inglis-Teller limit, where the mixing between levels of different principal quantum numbers is small, the averaging procedure minimizes the field distortion effect. Such averaging is physically reasonable whenever the l-changing collisions of the system with plasma electrons are rapid. However, when the typical transition rates for the state p are as large as the l-mixing collisions, the explicit l dependence and the field effect can be sizable.

(3) We have also stressed the fact that the definition of the effective rates α and S depends explicitly on the approximate rate equations one solves, in which the rates are to be inserted. This trivial but important point has been illustrated in Sec. IV, where the rates one generates correctly reflect the conditions under which rate equations are constructed.

The present study raises many questions which are yet to be clarified, such as (i) the l and field dependence of the system, both in the rate equations and rate coefficients; (ii) the time dependences of the electron and ion densities, and their relationship to the initial conditions; (iii) the presence of heavier impurity ions which can undergo many additional reactions involving more than one electron, such as dielectronic recombination; and (iv) possible nonequilibrium conditions on the electron and ion distribution, which can seriously affect the rates themselves. These questions will be examined in follow-up reports [17,18].

ACKNOWLEDGMENT

This work was supported by the Division of Chemical Sciences, Offices of Basic Energy Sciences, Office of Energy Research, U.S. Department of Energy.

APPENDIX A: ONE-LEVEL ATOMS

The model consists of the ground-state level 1 plus the continuum c i.e., $1+c$. The rate equation is simply given by

$$\dot{P}_1=-P_1n_cK_{1c}+n_cK_{1c}+(n_c^2/n_1^E)\beta_1 \equiv -S_1^{(1)}n_cP_1+\alpha_1^{(1)}(n_c^2/n_1^E) . \quad (A1)$$

Thus, we have

$$S_1^{(1)}=K_{1c}=S_{1c}^{(1)} , \quad (A2)$$

$$\alpha_1^{(1)}=\beta_1+(n_1^E/n_c)K_{1c}=\alpha_{1c}^{(1)}+\alpha_{1r}^{(1)} . \quad (A3)$$

The effective rates obtained by this simple model are given in Table IV. The model is simple and the change in $\alpha_1^{(1)}$ is noticeable immediately. Except for the collisional recombination rate α_1 at high density and high temperature, all the other values are essentially unchanged from the bare K_{1c} and β_1.

TABLE IV. The rates obtained for the one-level model of Appendix A. The shift in the dominance at high density, from r to c, is clearly seen. Numbers in square brackets denote powers of 10.

$\log_{10}n_c$	T (10^3 K)	$S_1^{(1)}$	$S_1^{(3)}$	S_1	$\alpha_1^{(1)}$	$\alpha_1^{(3)}$	α_1
8	4	1.3[−26]	4.2[−24]	1.1[−26]	2.5[−13]	5.3[−11]	9.8[−13]
8	16	3.4[−13]	1.5[−12]	3.6[−13]	1.2[−13]	4.2[−13]	3.1[−13]
8	64	1.5[−09]	2.4[−09]	1.6[−09]	5.2[−14]	9.6[−14]	1.0[−13]
13	4	1.3[−26]	4.5[−24]	2.5[−25]	2.5[−13]	5.7[−11]	1.3[−11]
13	16	3.4[−13]	1.6[−12]	1.1[−12]	1.2[−13]	4.4[−13]	6.3[−13]
13	64	1.5[−09]	2.4[−09]	2.4[−09]	5.2[−14]	8.6[−14]	1.2[−13]
18	4	1.3[−26]	1.1[−21]	8.2[−22]	3.3[−12]	2.7[−07]	2.0[−07]
18	16	3.4[−13]	2.2[−11]	2.3[−11]	1.5[−12]	9.4[−11]	9.7[−11]
18	64	1.5[−09]	8.1[−09]	8.8[−09]	5.2[−13]	2.6[−12]	2.9[−12]

TABLE V. The rates obtained with the two-level system of Appendix B. The strong effect of $P_2=1$ is demonstrated. The two different sets of solutions with labels (a) and (b) corresponding to the cases (i) and (ii) of Appendix B are presented. Numbers in square brackets denote powers of 10.

$\log_{10}n_c$	T (10^3 K)	$S_1^{(2)}$ (b)	$S_1^{(2)}$ (a)	S_1	$\alpha_1^{(2)}$ (b)	$\alpha_1^{(2)}$ (a)	α_1
8	4	1.3[−26]	4.8[−21]	1.1[−26]	3.8[−13]	6.0[−08]	9.8[−13]
8	16	3.4[−13]	2.2[−11]	3.6[−13]	1.8[−13]	4.7[−12]	3.1[−13]
8	64	1.5[−09]	7.4[−09]	1.6[−09]	7.2[−14]	1.4[−13]	1.0[−13]
13	4	1.4[−26]	4.8[−21]	3.6[−25]	3.9[−13]	6.0[−08]	1.3[−11]
13	16	3.5[−13]	2.2[−11]	1.1[−12]	1.8[−13]	4.7[−12]	6.3[−13]
13	64	1.5[−09]	7.4[−09]	2.4[−09]	7.2[−14]	1.4[−13]	1.2[−13]
18	4	1.5[−24]	4.8[−21]	8.0[−22]	3.5[−10]	1.2[−06]	2.0[−07]
18	16	1.3[−11]	2.2[−11]	2.3[−11]	5.3[−11]	2.1[−10]	9.7[−11]
18	64	7.0[−09]	7.4[−09]	8.8[−09]	2.3[−12]	2.7[−11]	2.9[−12]

APPENDIX B: TWO-LEVEL ATOMS

The second simple model is described in terms of levels 1 and 2 plus the continuum c, i.e., $1+2+c$. The corresponding rate equations are identical to (8), with $P_3=0$. Two different assumptions may be made on P_2.

(i) $P_2=1$. This gives immediately

$$\begin{aligned}\dot{P}_1 &= -P_1[n_cK_{1c}+n_cK_{12}]+n_cK_{12} \\ &\quad +(n_2^E/n_1^E)A_{21}+n_cK_{1c}+(n_c^2/n_1^E)\beta_1 \\ &\equiv -P_1n_cS_1^{(2)}(\mathrm{a})+\alpha_1^{(2)}(\mathrm{a})(n_c^2/n_1^E)\ , \end{aligned} \tag{B1}$$

which defines the effective ionization and recombination rates as

$$\alpha_1^{(2)}(\mathrm{a})=[\beta_1+n_cK_{21}]+(n_2^E/n_c^2)[A_{21}+n_cK_{21}]\ , \tag{B2a}$$

$$S_1^{(2)}(\mathrm{a})=K_{1c}+K_{12}\ . \tag{B2b}$$

The numerical values for the effective rates are given in Table V.

(ii) Alternatively, we may put $\dot{P}_2=0$, rather than the assumption $P_2=1$. The results of these two assumptions are given in Tables V, $S_1^{(2)}$(b) and $\alpha_1^{(2)}$(b). It clearly shows the effective of assuming $P_2=1$. At equilibrium $P_2=1$ gives generally an overestimation of the effect of the coupling. This is also true with the three-level model, but with less drastic effect. The more accurate model considered in Secs. II and III retains this feature.

[1] Y. Hahn, in *Recombination of Atomic Ions,* Vol. 296 of NATO Advanced Science Institute, Series B: Physics, edited by W. Graham *et al.* (Plenum, New York, 1992) p. 11.

[2] D. R. Bates, A. E. Kingston, and R. W. P. McWhirter, Proc. R. Soc. London, Ser. A **267**, 297 (1962); D. R. Bates and A. E. Kingston, Planet. Space Sci. **2**, 1 (1965); D. R. Bates and A. Dalgarno, *Atomic and Molecular Processes,* edited by D. R. Bates (Academic Press, New York, 1962), p. 245.

[3] L. C. Johnson and E. Hinnov, J. Quant. Spectrosc. Radiat. Transfer, **13**, 333 (1973); H. W. Drawin and F. Emard, Physica B+C **85**, 333 (1977); Z. Phys. **243**, 326 (1971).

[4] K. LaGattuta and Y. Hahn, Phys. Rev. Lett. **51**, 558 (1983); K. LaGattua, I. Nasser, and Y. Hahn, J. Phys. B **20**, 1565 (1987); **20**, 1577 (1987); Y. Hahn and K. LaGattuta, Phys. Rep. **166**, 195 (1988).

[5] G. H. Dunn, *Electron and Atomic Collisions,* edited by D. C. Lorentz *et al.* (North-Holland, Amsterdam 1986), p. 23; A. Muller, *Physics of Electronic and Atomic Collisions,* edited by A. Dalgarno *et al.* (AIP, New York, 1990), p. 418; D. R. Belic *et al.*, Phys. Rev. Lett. **50**, 339 (1983).

[6] B. Mitchell *et al.*, Phys. Rev. Lett. **50**, 335 (1983).

[7] P. Dittner *et al.*, Phys. Rev. Lett. **51**, 31 (1983).

[8] P. Krstic and Y. Hahn, Phys. Rev. A (to be published).

[9] L. P. Pitaevski, Zh. Eksp. Teor. Fiz. **42**, 1326 (1962) [Sov. Phys.—JETP **15**, 919 (1962)]; A. V. Gurevitch and L. P. Pitaevski, Zh. Eksp. Teor. Fiz. **46**, 1281 (1964) [Sov. Phys. JETP **19**, 870 (1964)].

[10] L. M. Biberman *et al.*, Usp. Fiz. Nauk **107**, 353 (1973) [Sov. Phys. Usp. **15**, 375 (1973)]; **22**, 411 (1979) [**128**, 233 (1979)]; L. M. Biberman, V. S. Vorob'ev, and I. T. Yakubov, *Kinetics of Nonequilibrium Low-Temperature Plasmas* (Consultant Bureau, 1987).

[11] A. Burgess and H. Summers, Astrophys. J. **157**, 1007 (1969).

[12] V. A. Godyak, R. B. Picjak, and B. M. Alexandrovich, Phys. Rev. Lett. **68**, 40 (192); V. A. Godyak and A. S. Khanneh, J. Phys. (Paris) Colloq. **40**, C7-125; **40**, C7-197 (1979).

[13] M. Baranger, Phys. Rev. **111**, 481; **111**, 494 (1958); in *Atomic and Molecular Processes,* edited by D. R. Bates (Academic Press, New York, 1962), Chap. 13.

[14] H. Griem, *Plasma Spectroscopy* (McGraw-Hill, New York, 1964); *Spectral Line Broadening by Plasmas* (Academic Press, New York, 1974); A. C. Komb and H. Griem, Phys. Rev. 111, 514 (1958).

[15] G. Peach, Adv. Phys. **30**, 367 (1981).

[16] Y. Hahn and P. Krstic, Phys. Scr. (to be published).

[17] J. Li and Y. Hahn (unpublished).

[18] J. Li and Y. Hahn (unpublished).

[19] H. A. Bethe and E. E. Salpeter, *Quantum Mechanics of One and Two Electron Atoms* (Springer-Verlag, Berlin, 1957).

[20] L. C. Greene, P. P. Rush, and C. D. Chandler, Astrophys. J. Suppl. **3**, 37 (1957).

[21] D. E. Post *et al.*, At. Data Nucl. Data Tables **20**, 397 (1977).
[22] Pengelly and M. Seaton, Mon. Not. R. Astron. Soc. **127**, 165 (1964).
[23] G. Flamond, J. Math. Phys. **7**, 1924 (1966).
[24] A. P. Stone, Proc. Cambridge Philos. Soc. **52**, 424 (1956).
[25] J. W. B. Hughes, Proc. Phys. Soc. London **91**, 810 (1967).
[26] Y. Hahn and P. Krstic (unpublished).
[27] K. Greenberg and G. A. Hebner (unpublished); P. J. Drallos and M. E. Riley (unpublished).